Airborne gravity and precise positioning for geologic applications

R. E. Bell, V. A. Childers,[1] R. A. Arko

Lamont-Doherty Earth Observatory of Columbia University, Palisades, New York

D. D. Blankenship

Institute for Geophysics, University of Texas, Austin

J. M. Brozena

Naval Research Laboratory, Washington, D.C.

Abstract. Airborne gravimetry has become an important geophysical tool primarily because of advancements in methodology and instrumentation made in the past decade. Airborne gravity is especially useful when measured in conjunction with other geophysical data, such as magnetics, radar, and laser altimetry. The aerogeophysical survey over the West Antarctic ice sheet described in this paper is one such interdisciplinary study. This paper outlines in detail the instrumentation, survey and data processing methodology employed to perform airborne gravimetry from the multi-instrumented Twin Otter aircraft. Precise positioning from carrier-phase Global Positioning System (GPS) observations are combined with measurements of acceleration made by the gravity meter in the aircraft to obtain the free-air gravity anomaly measurement at aircraft altitude. GPS data are processed using the Kinematic and Rapid Static (KARS) software program, and aircraft vertical acceleration and corrections for gravity data reduction are calculated from the GPS position solution. Accuracies for the free-air anomaly are determined from crossover analysis after significant editing (2.98 mGal rms) and from a repeat track (1.39 mGal rms). The aerogeophysical survey covered a 300,000 km² region in West Antarctica over the course of five field seasons. The gravity data from the West Antarctic survey reveal the major geologic structures of the West Antarctic rift system, including the Whitmore Mountains, the Byrd Subglacial Basin, the Sinuous Ridge, the Ross Embayment, and Siple Dome. These measurements, in conjunction with magnetics and ice-penetrating radar, provide the information required to reveal the tectonic fabric and history of this important region.

1. Introduction

Airborne magnetic surveys have long been a primary tool for geologic mapping, resource exploration, hazard evaluation, and tectonic studies. Over the last decade, advances in precise positioning have enabled other geophysical tools such as gravity meters and laser and radar altimeters to be effectively mounted on aircraft. The principle advantages of airborne geophysical surveys over ground-based studies result from enhanced experiment design, including improved access to remote and otherwise inaccessible areas, optimized sampling, rapid sampling rate, and tremendous potential for interdisciplinary studies.

Ground-based geophysical studies are often limited to sampling along roads and trails. An airborne experiment enables the scientist to optimally design the survey to address the study targets without limitation of ground access. The selec-

tion of line spacing in an airborne survey can be based solely on the desired geologic resolution with minimum consideration for topography, vegetation, and cultural features. The ability to select both the desired line spacing and flight elevation often results in more accurately sampled and better resolved anomalies than those produced from land-based data.

An additional advantage of aerogeophysics is the rapid rate of airborne data acquisition. For example, during a single Antarctic field season, an airborne gravity survey covered an area 110,000 km² with orthogonal lines spaced 5 km over the course of 56 days. A surface-based survey of the area, using snowmobiles and highly trained mountaineering teams to cross heavily crevassed regions, would have taken in excess of 12 months with four gravity meters. The airborne system clearly provides faster data acquisition and a generally safer field method. The rapid data acquisition provided by an airborne system has been well documented in mountainous, coastal, and tropical regions [*National Research Council*, 1995].

As precise positioning is critical to the recovery of high resolution airborne gravity, differential Global Positioning System (GPS) positioning techniques have been the key to expanding usage of airborne gravimetry. Initial airborne gravity experiments in the late 1950s failed to recover short wavelength geologic structures due to the difficulty of accurately

positioning the aircraft. The advent of precise positioning via GPS satellites opened the door to increasingly broad applications of airborne gravity. Early experiments used solely GPS pseudorange positions [*Bell et al.*, 1990; *Brozena*, 1984] and were limited to over-water applications where the vertical position of the aircraft could be recovered with ranges to the sea surface. The development of differential carrier phase techniques has opened up continental areas to study with airborne gravity [*Brozena*, 1995; *Brozena et al.*, 1989; *Gumert*, 1995; *Harrison et al.*, 1995]. The goal of this paper is to describe the airborne gravimetry and the associated precise positioning techniques developed as part of an integrated aerogeophysical research platform developed for polar applications.

2. Aerogeophysical Survey Operation

2.1. Instrumentation of the Aircraft

The Antarctic airborne gravity system is part of a Twin Otter instrumented to acquire multiple data types simultaneously (Plate 1). The primary geophysical systems are the airborne gravity system, a towed aeromagnetic system, an ice-penetrating radar, and a laser altimeter. The experimental goal of the aircraft is to recover Bouguer and free-air gravity anomalies, accurate magnetic anomalies, sub-ice topography, and accurate delineation of the ice surface. Positioning and navigation instrumentation includes a laser-ring gyro inertial navigation system, a pressure altimeter, a real-time differential GPS navigation system, a dual GLONASS/GPS receiver, and a suite of carrier phase GPS receivers (GLONASS is the Russian Global Navigation Satellite System). The aircraft instrument suite is supported by base station instrumentation including a base magnetometer to remove the diurnal magnetic signal, a stationary GPS with a broadcast system transmitting the differential GPS correction, and dual-frequency carrier phase GPS receivers. The positional accuracies required for the various instruments are shown in Table 1 and the accuracy of the positioning systems in Table 2.

The gravity instrumentation has included both a Bell Aerospace BGM-3 gravity meter and a LaCoste & Romberg "S" gravity meter modified by ZLS Corporation. Early comparison of the airborne data with surface data collected along the Horlick Mountain Traverse route suggested that anomalies with wavelengths of as little as 5 km and with accuracies of better than 5 mGal can be recovered from the airborne gravity system mounted on the Twin Otter [*Bell et al.*, 1991; 1992]. Early evaluation of the fully gridded data suggested a resolution of 5 km with an accuracy of 2.7 mGal [*Brozena et al.*, 1993].

Radar mapping of ice thickness is crucial to glaciologic studies while the tracing of the bedrock topography is critical to understanding the tectonic fabric of a region and for calculation of the Bouguer gravity anomalies. The radar, developed jointly by the National Science Foundation (NSF) and the Technical University of Denmark (TUD) [*Skou and Sondergaard*, 1976], transmits a peak power of 10 kW on a carrier frequency of 60 MHz. This radar system, used to collect profiles flown over East and West Antarctica from a LC-130 transport aircraft in the 1970s, was modified to fit a DeHavilland Twin Otter. The digitally recorded NSF/TUD radar can penetrate over 3000 m of warm West Antarctic ice and an even greater thickness of cold East Antarctic ice.

Owing to the importance of the surface slope for glaciologic studies and the ice surface for gravity measurement, accurate mapping of the ice surface is a key objective.

The geophysical Twin Otter aircraft has been instrumented with a Holometrix Pram IV laser altimeter with a ranging accuracy of 0.1 m. This laser altimeter has a footprint of about 0.9 m with averaged range data recorded about every 10 m along track. Off-nadir attitudes of the aircraft are corrected with the pitch and roll angles recorded by the inertial navigation system.

Aeromagnetic data are used in conjunction with the gravity anomalies to document the regional tectonic fabric. The Twin Otter magnetic system utilizes a proton-precession magnetometer (a Geometrics 813) with observations acquired every 60 m with an estimated precision of about 1 nT. During the field season, magnetic base stations are operated in the field camp to monitor the changing magnetic field during the survey.

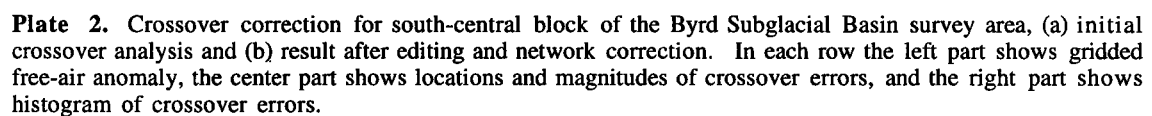### 2.2. Survey Design and Location

The survey is designed to produce the optimum data set for each of the four primary geophysical measurements in light of the restrictions imposed by the multi-instrument platform. For example, the airborne gravity data are optimized when the aircraft is flown at a constant altitude above sea level, while the ice-penetrating radar measurement is optimized by acquiring the data as close to the ice surface as possible. The laser ranges to the ice surface can only be recovered in cloud-free conditions which cannot be guaranteed if the survey is collected at a constant elevation. The survey design represents a compromise for each of the systems. The area is covered by a grid of orthogonal survey lines spaced 5.3 km apart in both directions. The orthogonal design also provides a large number of crossovers for identifying discrepancies in the airborne data. The aircraft elevation is constant for each 110 by 110 km square region with a minimum clearance of 300 m above the estimated terrain. Twenty four of these 110 by 110 km regions were surveyed over the West Antarctic ice sheet over the course of 5 field seasons, encompassing an area of 300,000 km^2 (Figure 1).

3. Precise Positioning

The precise positioning demands of an airborne gravity system require that a differential GPS positioning strategy be employed. Pseudorange positions from a single receiver aboard the aircraft do not provide sufficiently accurate positions to recover airborne gravity. The differential strategy requires the continuous operation of a fixed receiver (at a base station) recording GPS data and the simultaneous acquisition of GPS data from a receiver aboard the aircraft. Differential processing techniques remove errors such as clock and satellite orbit errors that are common to both receivers. As pseudorange and carrier phase data are acquired from the GPS systems both in the aircraft and in the base station, a differential position can be calculated from either the pseudorange data or the carrier phase data. Of the two positioning solutions, the differential carrier phase is inherently superior. The phase of the carrier wave can be measured more precisely than the pseudorange observable, and the carrier measurement is less affected by multipath and by ionospheric and tropospheric delays.

3.1. Instrumentation and Field Operation

The Antarctic differential GPS system includes a minimum of two carrier phase receivers installed in the Twin Otter and a minimum of three receivers at the base stations. The GPS in-
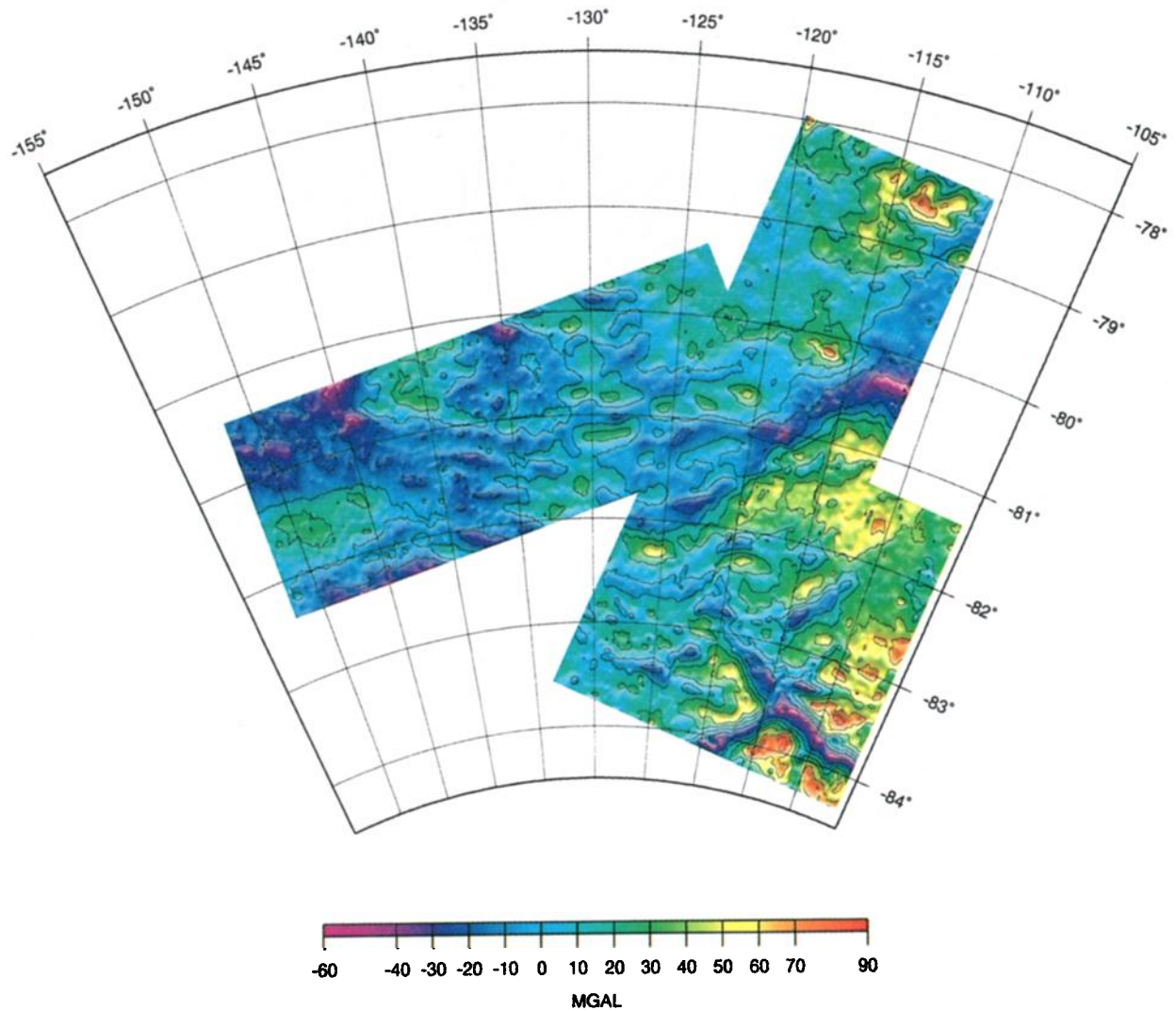
PRESSURE
WAND

RADAR
ANTENNA

MAGNETOMETER
"BIRD"

Plate 1. The ski-equipped Twin Otter aircraft instrumented for the aerogeophysical survey. The gravimeter is installed inside at the aircraft's center of gravity.

Plate 2. Crossover correction for south-central block of the Byrd Subglacial Basin survey area, (a) initial crossover analysis and (b) result after editing and network correction. In each row the left part shows gridded free-air anomaly, the center part shows locations and magnitudes of crossover errors, and the right part shows histogram of crossover errors.

GRAVITY FREE-AIR ANOMALY

Plate 3. Free-air gravity anomaly map for the West Antarctic survey. The physiographic features of the region are clearly expressed in the gravity field. The location of the survey is shown in Figure 1.

Table 1. Positional Accuracies Required for Twin Otter Geophysical Systems

Measurement	Horizontal	Vertical
Ice-penetrating radar	10-20 m	2.5 m
Surface altimetry	5-10 m	0.5 m
Airborne gravity	30 m 0.1 m s^{-1} (velocity)	2 m and 0.1 m (relative) 1×10^{-5} m s^{-2} (acceleration)
Aeromagnetics	30 m	10 m

between position calculated from carrier phase and position calculated from pseudorange), and ionosphere cycle-slip detection cutoff (the difference in ionospheric correction between consecutive epochs). Adjusting parameters always involves trade-offs. For example, lowering the satellite elevation cutoff below its normal value of 15° allows initialization of a satellite earlier in its ascent (and retention of lock later into its descent), but there is a greater risk of atmospheric interference when a satellite is low on the horizon.

Solutions are calculated starting from the beginning of the flight until after the end of the final survey line. To evaluate the quality of a completed solution, we plot time series of the root mean squared error estimate and the relative dilution of precision (RDOP) (an estimate of the quality of the satellite geometry). An "adequate" solution has an rms error estimate below 0.04 m for the duration of the flight. If the rms error estimate deteriorates at some point, either a satellite was improperly initialized or a cycle slip occurred but was not detected. In either case, the solution parameters are adjusted to achieve a good solution.

Occasionally, the differential carrier phase data are incomplete, and an alternative positioning technique must be used to recover the gravity data from a flight. During early field seasons when operations depended heavily on a single type of GPS receiver, a large percentage of carrier phase solutions (up to 30%) were lost. Recent field seasons have relied more heavily on Ashtech receivers, and recovery of carrier phase solutions has improved dramatically (less than 5% lost). Differential pseudorange solutions provide the next best positions. The differential pseudorange, although superior to the raw pseudorange, is still degraded by multipath as well as by ionospheric and tropospheric delays. Pressure altimetry provides an alternative source for vertical positions but is limited in its recovery of absolute altitudes, particularly when flight lines cross isobars.

To evaluate the error associated with alternative position measurements, we calculated the free-air gravity anomaly for nine lines using three positioning techniques: (1) differential carrier phase, (2) differential pseudorange, and (3) differential pseudorange for horizontal positions and pressure altimetry for vertical positions. We assumed that the differential carrier

phase solution best approximates the actual aircraft position and evaluated the difference between this position and the other positioning methods. The initial statistical comparison indicates little difference between the methods for the purpose of calculating vertical acceleration, with the differential pseudorange and pressure altimeter yielding cumulative errors of 3.66 and 2.87 mGal rms, respectively. For the purpose of calculating the free-air correction, the differential pseudorange and pressure altimeter yield cumulative errors of 0.17 and 2.23 mGal rms, respectively. The clearest evidence in favor of the differential pseudorange, however, is in the power spectrum. As shown in Figure 2, the power spectral density estimate for the aircraft's vertical acceleration as calculated using the differential pseudorange approximates the carrier phase much more closely than the pressure altimeter approximates it. Thus our data reduction strategy is to use differential pseudorange positions when carrier phase positions are not available.

In general, the quality of the GPS carrier phase solution is a function of the number of satellites visible, the geometry of their positions in the sky, the baseline distance between the aircraft and the base station, and the multipath environment of the GPS antenna mounted atop the aircraft fuselage. At high latitudes, the quality of the solution is further degraded by increased ionospheric interference and low satellite elevation.

A potentially important source of error in the carrier phase solution is associated with the acquisition and loss of satellites. Satellites acquired mid-flight during periods of poor geometry or long baselines can be difficult to initialize correctly. An incorrect bias creates a positioning error that grows with time, causing the solution to "drift." The loss of a satellite from the least squares solution can cause a discrete step in the vertical positioning, which can translate into a significant error in the free-air anomaly.

One approach to quantify the errors associated with satellite loss and initialization is to examine in detail two GPS solutions for a single flight, one with biases initialized at the beginning of the flight and the solution processed "forward" in time, and the other with biases fixed at the end and processed with time "reversed." The timing of satellite initialization and loss can significantly differ between the forward and reverse solution, thus the arithmetic difference between the vertical
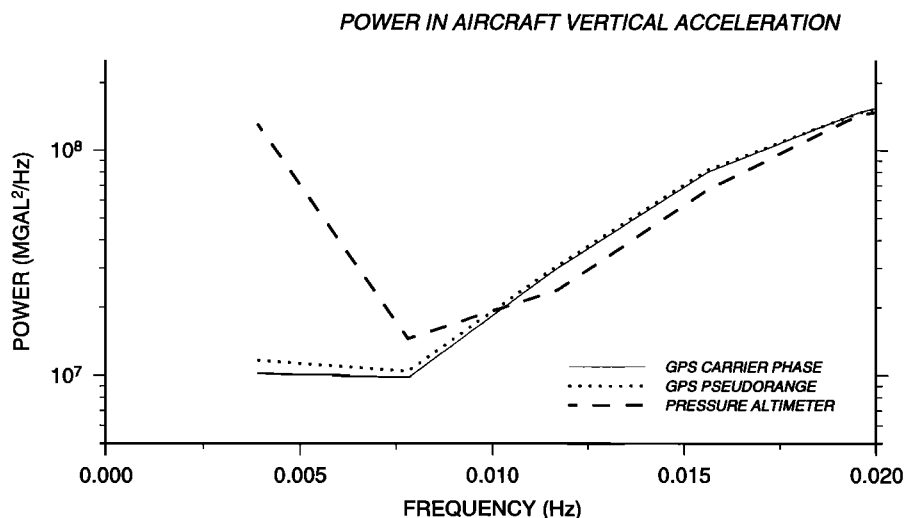
POWER IN AIRCRAFT VERTICAL ACCELERATION

Figure 2. Power spectral density estimate for the aircraft's vertical acceleration, as calculated using GPS carrier phase, differential pseudorange, and pressure altimeter.

positions of the two solutions should highlight the errors in either one and provide an estimate of the maximum potential error introduced by the changing constellation within the GPS solution. We evaluate the error in aircraft altitude and the filtered accelerations that these positioning errors would introduce into the free-air anomaly for a flight characterized by good rms and RDOP values (Figure 3). The section of the flight we have examined (Figure 3) is characterized by an overall zero mean in the differenced positions superimposed with noisy spikes of amplitude 10-57 cm lasting from 5 to 250 s and a distinct step in aircraft position of 18 cm at 500 s. The spiky differences represent periods where noisy ionosphere caused a cycle slip to be identified where none was present. These "noisy" periods occurred while the questionable satellite was removed from the solution, while its bias was again determined by the integer search algorithm. The difference returns to zero once the bias is redetermined and the satellite is again included in the solution. For events with a zero mean, such as those after 1700 s, the maximum effect of the noise on the filtered vertical acceleration, and thus on the free-air anomaly, is about 0.5 mGal.

The most significant error was introduced when a satellite bias was determined incorrectly by one cycle in the reverse solution following an erroneous cycle slip. This error was corrected 2 min later, but the resulting 18 cm step in the height solution translated into an error of 3 mGal in the filtered vertical acceleration with a wavelength of ~21 km (300 s). The extensive periods of zero difference and zero mean between the two solutions indicate correct bias initialization for both solutions with no appreciable accumulating error in either solution.

4. Airborne Gravity Measurement

4.1. Gravimeter System

A Bell Aerospace BGM-3 gravimeter forms the basis of the Twin Otter airborne gravimetry system. The sensor is a Bell Model XI inertial-grade accelerometer [*Bell Aerospace Textron*, 1978]. A proof mass, constrained to only move in the vertical direction, is maintained at a null position in an electromagnetic field. The current required to null the proof mass
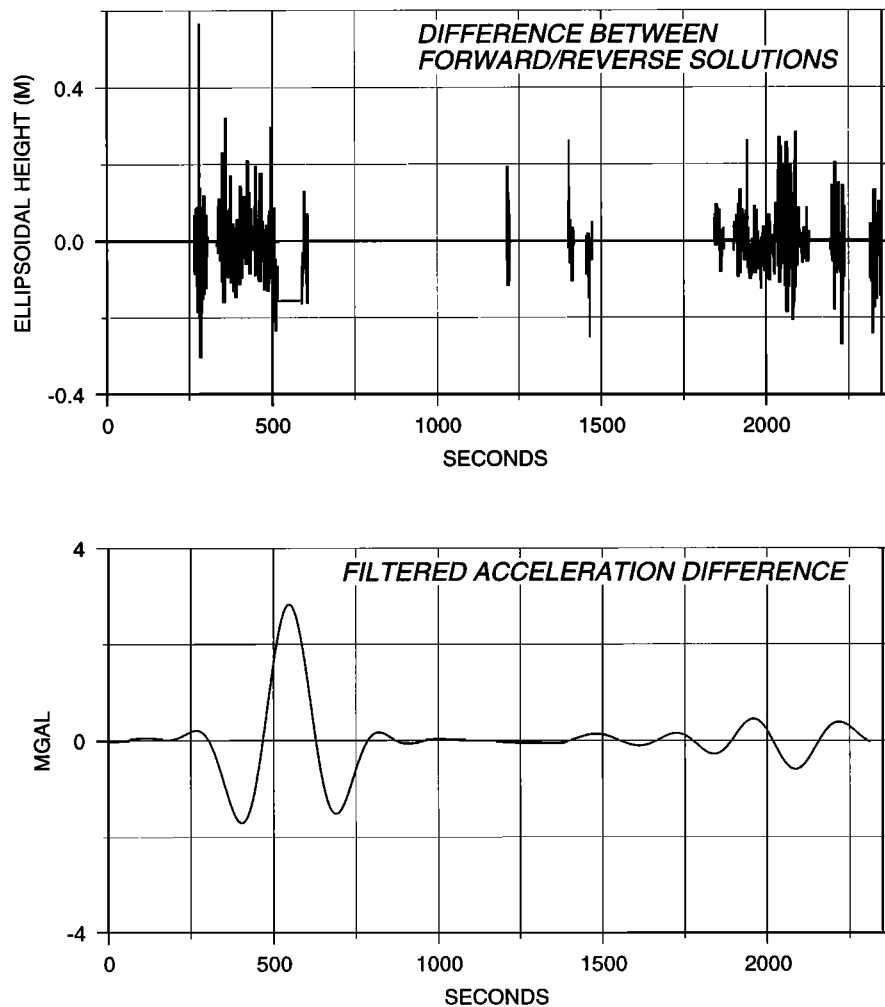
Figure 3. The arithmetic difference between a forward and a reverse Global Positioning System carrier phase solution for a survey line is shown. Non-zero values indicate periods where the solutions differ, highlighting periods where changing satellite geometry in the Global Positioning System solution degrades one or the other solution. The step just after 500 s represents the worst problem in this line, when the Kinematic and Rapid Static program incorrectly reinitialized a satellite during a period of noisy ionosphere then corrected the bias about 2 min later.

varies linearly with the accelerations experienced by the sensor. The varying current in the restoring coil is digitized and summed over 1 s intervals.

A LaCoste and Romberg (L&R) S meter upgraded by the ZLS Corporation to include digital platform control and variable platform period was used during one season. The L&R model S gravity meter sensor consists of a proof mass mounted at the end of a highly damped, pivoting beam supported by a specially designed spring. The acceleration measurement comprises the spring tension, the velocity of the beam, and a cross-coupling correction to account for coupling of horizontal motions into the vertical measurement.

For both gravimeters, the sensor is mounted on a two-axis, gyro-stabilized platform that aligns the sensitive axis of the accelerometer with the time-averaged local vertical. Orthogonally oriented gyros and accelerometers serve to align the platform with the geoid in the absence of horizontal accelerations. In the presence of horizontal accelerations, the platform aligns to the total acceleration vector, the resultant of the local horizontal and vertical accelerations. High-amplitude horizontal accelerations, such as those associated with a course correction, can cause the vector to sufficiently deviate from the vertical to introduce error into the measurement. The BGM-3 platform erection loop corrects for these errors at laboratory-induced acceleration periods, although the correction is untested at periods longer than 20 s (L. Meister, Bell Aerospace, personal communication, 1996).

The gravimeters are relative instruments, measuring the change in gravity with respect to a reference value. We determine the relationship between the gravimeter measurement and the absolute measurement through the gravity tie. The nearest International Gravity Standardization Network (IGSN-71) reference station to our field camp is located at McMurdo Station (monument BLDG57, position 77.8477°S - 166.6820°E, elevation 35.1 m, absolute value 982972.72 mGal). Gravity was measured at both BLDG57 and at a fixed monument in each field camp with a portable land meter, which allowed us to calculate a reference value for the field monument. A reading was then taken from the aircraft gravimeter at that monument, prior to installation in the aircraft. The difference between the reference value and the observed value from the gravimeter (the "tie" value) was applied to all meter observations made while the aircraft was deployed from that field camp. Tie values are summarized in Table 3.

The gravimeter is mounted at the center of gravity of the aircraft. The BGM-3 platform enclosure is bolted to the floor, and the sensor is shielded from vibration by rubber shock mounts within the platform assembly. Ovens maintain the sensor and the platform gyros at a constant temperature to en-

hance meter performance. For the L&R meter, the platform is shock-cord suspended to prevent transmission of vibrations to the sensor. Additionally, an insulated wooden box surrounds each meter to buffer temperature extremes inside the aircraft.

The gravimeter measurement is recorded by the data acquisition computer at a 1 Hz rate, with a time assigned to each measurement by an internal time standard. Data recording begins when the aircraft is steady on track and continues until just before the aircraft turns to align with the next track. The tracks are extended 15 km on both ends to ensure high quality data within the target area and sufficient overlap between the survey blocks.

4.2. Data Reduction

Throughout the field season, the data are routinely evaluated to verify that all systems are functional and are performing well. After each flight, the gravity data are examined for consistency in the time intervals between measurements and to identify any data losses. A preliminary free-air gravity anomaly is calculated using the differential pseudorange solution for horizontal positioning and the pressure altitudes for vertical positioning. This preliminary anomaly should show gravity values that are smoothly varying within a reasonable range, with a high correspondence between neighboring profiles.

In postseason processing, once the carrier phase positions are calculated using precise ephemerides, corrections derived from the latitude, longitude, and ellipsoidal height of the aircraft are applied to the gravity measurement to generate the free-air gravity anomaly. Acceleration of the aircraft along the vertical (A_{vert}) must first be calculated and subtracted from the gravimeter measurement ($A_{measured}$). Of all corrections calculated, correct determination of the aircraft's vertical acceleration is the most crucial to achieve a high-quality, free-air anomaly. The second difference of the GPS carrier phase aircraft heights provides the preferred estimation of vertical acceleration. There is substantial similarity in waveform and amplitude between the gravimeter measurement and the vertical acceleration, as highlighted by a comparison of these filtered quantities for a survey line (Figure 4). The Eötvös correction for airborne measurements is calculated to compensate for measuring gravity from a moving platform on a rotating Earth [*Harlan*, 1968] and is added to the measurement. The anomalous gravity is determined by then subtracting the predicted gravity for that latitude at the ellipsoid (G_{theo}) and adding the free-air correction (FAC) to correct the predicted gravity to the altitude of the aircraft (Figure 4). These corrections combine to yield the free-air anomaly (FAA).

$$FAA = A_{measured} - A_{aircraft} + Eötvös + FAC - G_{theo} \qquad (1)$$

Table 3. Gravity Tie Values

Field Camp (Monument)	Position	Elevation, m	Land Meter, mGal	Aircraft Meter, mGal	Tie, mGal
CASERTZ (CTZ)	82.3595 °S 118.1307 °W	1050	982780.72	982743.90	36.82
Byrd Surface Camp (NBY)	80.0080 °S 119.5607 °W	1505	982592.49	982546.73	45.76
Siple Dome (SDM)	81.6537 °S 149.0027 °W	626	982906.02	982873.59	32.43

OBSERVED GRAVITY

982240
982220
982200
982180
982160

VERTICAL ACCELERATION

40
20
0
-20
-40

EÖTVÖS CORRECTION

280
260
240
220
200

FREE-AIR CORRECTION

640
620
600
580
560

FREE-AIR ANOMALY

20
0
-20
-40
-60

MGALS

0   400   800   1200   1600   2000   2400
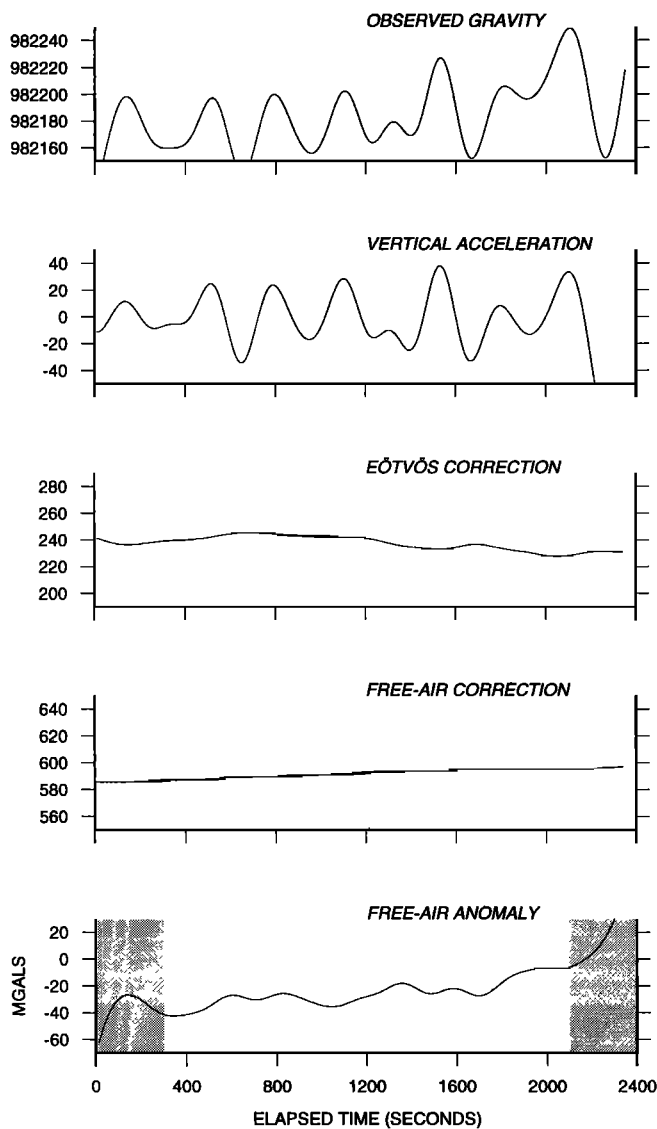
ELAPSED TIME (SECONDS)

Figure 4. The raw gravimeter measurement is shown along with the corrections required to produce the free-air gravity anomaly, all low-pass filtered. Note the similarity in waveform and amplitude of the gravimeter measurement and the vertical acceleration. The ends of the free-air anomaly must be trimmed to remove filter artifacts (gray shaded region).

The gravimeter measurement and the aircraft vertical acceleration data can be characterized as broadband signals with high amplitudes at high frequencies. Gravimeter data often range as much as +/-20,000 mGal about the mean for a typical survey line. Power spectral estimates of the gravimeter data (Figure 5) indicate that the power reaches a maximum by 0.03 Hz (33 s period) and remains high at the Nyquist frequency of 0.5 Hz. Aggressive low-pass filtering is required to minimize the high amplitude noise that remains in the free-air anomaly even after the corrections are applied. Noise attenuation is optimized by a cosine taper applied as a filter in the frequency domain that begins its roll off at 0 Hz (dc) and reaches infinite attenuation at 0.006 Hz (Figure 5). This filter passes the long wavelength gravity anomalies with only slight attenuation, while the higher frequency noise is completely attenuated.

After the processing of the free-air anomaly is complete, the profile is edited to remove the first and last 200 s corrupted by the filter, and, if necessary, to remove data at the ends of the lines where the aircraft turn contaminates the gravity measurement (Figure 4). At the beginning of a line, data contamination can occur when data recording begins before the gravimeter has had adequate time to equilibrate after a turn. If recording continues into a turn at the end of the track, this segment must also be removed. For the 44 profiles which comprise survey block BSB/SC (Byrd Subglacial Basin, South Central), we discarded 7.5% of the initial profile data in order to eliminate these filter and/or equilibration effects.

Once a complete set of profiles for one block has been reduced, we combine them and calculate crossover errors at profile intersections using the algorithm from *Wessel* [1989]. Sections of profiles with large crossover errors are removed. A dc shift and drift rate (i.e., best-fit regression line) is calculated for each profile that minimizes the overall standard deviation for the block in a least squares sense. The dc shift and drift rates are then applied to the profiles, and the data set is gridded using a spline function [*Smith and Wessel*, 1990]. We continue to remove sections of profiles with large crossover errors and recalculate the dc/drift corrections until a standard deviation of less than 3 mGal is achieved for the block. An additional 3.7% of the profile data was removed from block BSB/SC during this editing phase, to achieve a standard deviation of 2.908 mGal. Plate 2 shows results for block BSB/SC before (Plate 2a) and after (Plate 2b) the profile editing and dc/drift corrections are applied.

The quality of airborne gravity data can be evaluated both by examining in detail the values of crossover errors and by examining data acquired along a single profile at different times. The two profiles are coregistered, and the amplitude and character of the difference is examined. In general, we have found the difference between two flights flown along a single profile is less than 3.0 mGal [*Childers*, 1996]. As the Twin Otter system operation improved, we found that the routine comparison between two flights was often better than 2 mGal. In Figure 6, profiles flown during two separate field seasons are compared. The flight characteristics of these two profiles are similar with both raw accelerations being in the range of +/- 20,000 mGal, although the 1996 flight experienced slightly higher aircraft pitch and roll values than the 1995 flight. The maximum horizontal separation of the profiles is 250 m. Given the maximum regional gravity gradient observed along the profile of 0.95 mGal/km, it is possible that only ~0.25 mGal is the result of the regional gravity difference. The rms difference between these two lines is 1.39 mGal although there seems to be some offset of the anomalies. Possible causes of this offset are errors in the GPS solutions and errors introduced from an off-level platform.

4.3. West Antarctic Gravity Data

The airborne gravity system described here has been used to acquire 150,000 line kilometers of airborne gravity data covering a 300,000 km² region in West Antarctic through the course of five field seasons. This area is slightly larger than the state of Texas. The resultant free-air gravity map reflects both the major topographic and geologic structures of the region covered by 200 to 3900 m of ice (Plate 3). As the radar data has proven more difficult to reduce than anticipated, no Bouguer anomaly map is presented here. Analysis papers which inte-
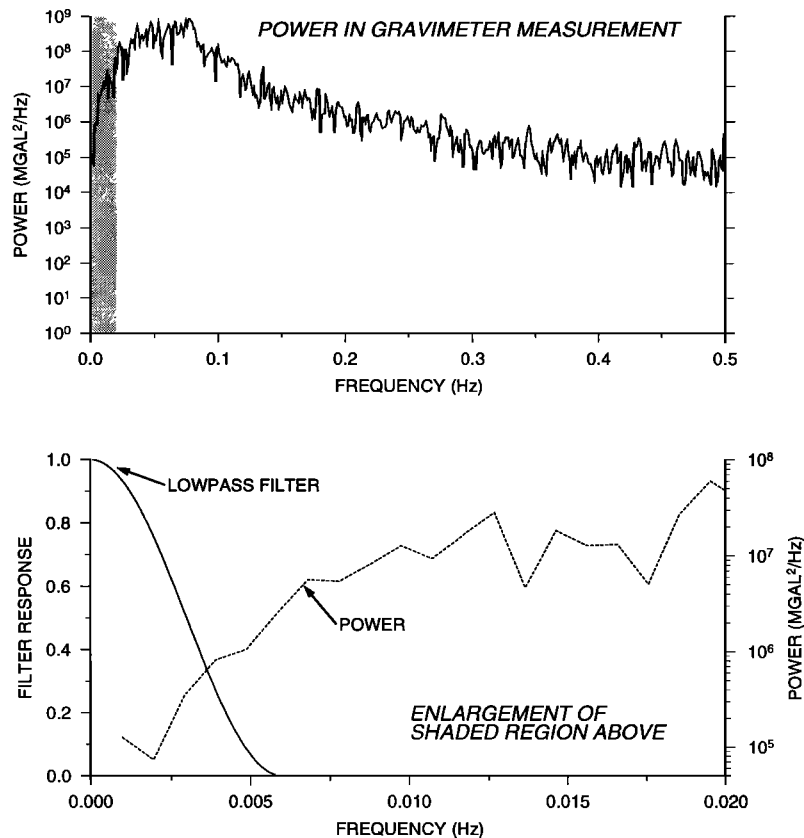
Figure 5. Power spectral density estimate for the raw gravimeter measurement for the survey line shown in Figure 3. Note that the power increases quickly with frequency and remains high at the Nyquist frequency. In Figure 5 (bottom) the frequency response of the low - pass filter used in the data reduction is superimposed upon an enlargement of the shaded region of Figure 5 (top).

grate the gravity, magnetics, and topography data will be forthcoming. The character of the gravity map changes dramatically from the high-amplitude gravity anomalies in the southeast to the broad, subdued anomalies characterizing much of the western portion. The range of the gravity map extends from a maximum of 82 mGal over a subglacial peak in the southwestern corner of the Whitmore Mountains to a minimum of -64 mGal over a deep subglacial trough of the Byrd Subglacial Basin.

The free air gravity map recovers a major portion of the West Antarctic rift system, a lithospheric structure comparable in size to the Basin and Range of western North America and the East African rift system. This rift system between East and West Antarctica may have been a site of frequent reactivation since the Paleozoic [*Wilson*, 1995], but the current rift system has formed principally as the result of extensional and translational plate motions beginning in the Jurassic during the fragmentation of Gondwana [*Behrendt et al.*, 1991; *Cooper et al.*, 1991; *Dalziel and Elliot*, 1982; *Wilson*, 1992]. Morphologically, the rift system consists of a broad low-lying region of extended crust bounded by elevated rift margins, the Transantarctic Mountains to the south and west and Marie Byrd Land to the north. The southern rift flank reaches from the edge of the Ross Sea over 3000 km along the Transantarctic Mountains incorporating the elevated crustal block of the Whitmore Mountains. This gravity survey reveals several of the major structures within the West Antarctic Rift system and the nature of the boundary between the rift system and the Whitmore

Mountains. The five major physiographic features reflected in the gravity map include the Whitmore Mountains, the southern portion of the Byrd Subglacial Basin, the elevated Sinuous Ridge which bisects the Byrd Subglacial basin, the thin low-lying crust of the Ross Embayment, and the elevated structure of Siple Dome.

The Whitmore Mountain region is characterized by rugged topography with elevations ranging from 250 m below sea level to Mt. Chapman at 2715 m, the sole outcrop covered by the survey. The gravity over this region ranges from +10 mGal to +80 mGal and reflects the rugged topography. The
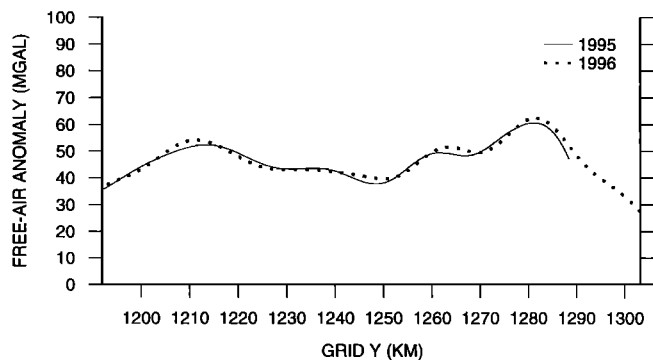

Figure 6. Two measurements of a survey line made in different seasons are shown. Root mean squared correspondence between the two lines is 1.39 mGal.

crust in this region is comprised of deformed Paleozoic sedimentary strata intruded by Middle Jurassic granitoids. The Whitmore Mountains are bounded by the Byrd Subglacial Basin to the north and by narrow linear gravity anomalies to the west and south.

The Byrd Subglacial basin is a deep, poorly defined feature extending from the Whitmore Mountains north toward Pine Island Bay. The basin is characterized by low-lying bedrock with elevations from 1000 m to more than 2500 m below sea level. The low gravity signature (-64 mgal) over the basin is indicative of the low elevations of the region. A highly magnetic sinuous structure, often referred to as the Sinuous Ridge, bisects the basin into a narrow, deep trough north of the Whitmore Mountains and an extensive area of subdued but deep topography continuing north toward Pine Island Embayment. The survey covers a portion of the Sinuous Ridge, a feature characterized by topographic elevations ranging from 1000 m below to 1000 m above sea level and gravity anomalies ranging from 18 to 83 mgal. The rugged nature of the gravity anomalies reflects the topography, indicating that this structure may not be a ridge as previously interpreted, but, in fact, a sequence of isolated peaks.

The Ross Embayment, is characterized by bedrock elevations that are primarily 500 m below sea level with deviations of the order of 200 m [*Drewry*, 1983; *Robertson et al.*, 1982; *Rose*, 1982]. The portion of the Ross Embayment covered with this survey is characterized by lineated gravity anomalies from -17 to +33 mGal with wavelengths ranging from 40 to 100 km. This region is overlain by the Ross ice sheet and many of West Antarctica's major ice streams. Lineated gravity anomalies correlate closely to the regional topographic trends that dominate the Interior Ross Embayment and have long been interpreted as sedimentary basins similar to those of the Ross Sea region.

Siple Dome, often interpreted as an elevated granitic block, is characterized by a distinctive gravity high ranging from 0 to 33 mGal. This corresponds to the elevated topography of the region with maximum elevations reaching 500 m below sea level.

4.4.   Resolution Analysis

The gravity data can be used to delineate fine scale features when integrated with the topography and magnetics, as illustrated in the identification of a subglacial sedimentary basin [*Bell et al.*, 1998] and a subglacial volcano [*Blankenship et al.*, 1993] with this data set. The limit in resolution of the data along a profile is a function of survey parameters, such as aircraft altitude (distance above anomaly source) and speed, and the amount of low-pass filtering required to attenuate the system measurement noise. The resolution of gridded data is also impacted by survey line spacing, with closer line spacing enhancing the spatial sampling of anomalies.

Aircraft distance above the source is the primary control on the amplitude and wavelength of anomalies observable from the aircraft platform. As aircraft altitude increases, anomaly amplitude falls off as $e^{-2\pi z/\lambda}$, where z is the distance to the source and λ is the wavelength of the anomaly. This effect is termed upward continuation [*Turcotte and Schubert*, 1982] and shorter wavelengths are attenuated preferentially as z increases. The shortest wavelength anomalies are generated by sources closest to the aircraft, such as the topography in overland flights or the bedrock interface in flights over ice sheets or water. For

the West Antarctic survey, aircraft elevations above the ice ranged from 300 to 900 m, and ice thickness varied from 200 to 1000 m over the Sinuous Ridge and up to 3900 m thick over the Byrd Subglacial Basin. Minimum observable anomaly wavelengths are predicted based upon the survey parameters of aircraft distance to source, aircraft speed (70 m/s), the density contrast at the rock/ice interface (1.2-1.65 x 10^3 kg m^{-3}), assuming a minimum anomaly amplitude of 2 mGal to be distinguishable from the measurement noise [*Childers*, 1996]. Where ice thickness ranges from 200 to 1000 m, minimum predicted anomalies range from 1.5 to 4 km half-wavelength. When the distance to the source dramatically increases over regions of thick ice, minimum wavelengths increase to 8-9 km half-wavelength.

The low-pass filtering required for noise attenuation places the definitive limit on the anomaly resolution. The cosine taper filter employed has its half-power point at 0.0022 Hz, corresponding to a period of 455 s, or 15 km half-wavelength at the average aircraft speed of 70m/s. Attenuation becomes infinite at 0.006 Hz, or 167 s, corresponding to 5.5 km half-wavelength, indicating that no smaller feature survives the filter. Because this frequency maps into wavelength according to aircraft speed, resolution is enhanced by slower speeds when these limiting frequencies result in shorter wavelengths. Overall for regions of thin ice (1000 m or less), the resolution is controlled by the severe filtering required by the airborne gravity measurement. In regions of thicker ice, the resolution is principally controlled by upward continuation and the distance to the source.

Airborne gravity is acquired in a dynamic environment that introduces substantial noise into the measurement. Noise in the free-air anomaly is attributed to uncorrected motion-induced error in the gravimeter measurement and errors in the precise GPS positions. Most noise in the gravimeter reading scales with the amplitude of aircraft motion, as has been shown by the correlation between gravimeter error and sea state in marine gravimetry [*LaCoste*, 1967]. Errors in the gravimeter measurement can be attributed to sensor and/or platform performance. Sensor errors would most likely occur if the dynamic range of the accelerometer is exceeded. The BGM-3 sensor has a dynamic range of ±0.1 g, which is rarely if ever approached in the Twin Otter. The dynamic range for the L&R sensor is ±1.0 g, sufficient for any airborne application. Platform behavior is the more likely source of errors because horizontal accelerations induced by course corrections can cause misalignment of the sensor with the local vertical. Offlevel corrections, calculated according to LaCoste's theory, only compensate for a portion of the total error introduced [*Childers*, 1996]. Long wavelength errors in the GPS positioning also contribute to errors in the gravity measurement. Static tests indicate that some noise exists at the longest wavelengths in the GPS vertical acceleration data (2-3 mGal at frequencies of DC to 0.0083 Hz) [*Peyton*, 1990], and additional noise that results from multipath in the airborne environment has not been quantified. No formal upward continuation was conducted on these data. The data were reduced to sea level using a simple free air correction. Some long wavelength errors may result from this treatment of the data.

5. Summary and Conclusions

This paper outlines the acquisition and reduction of airborne gravity for a regional interdisciplinary study. The airborne

gravity data recovered in the study of West Antarctica effectively outlines the major tectonic terrains of the regions and the nature of the boundaries between them. As global satellite missions are launched, airborne gravity will fill a unique niche for studies where data cannot be acquired effectively at the Earth's surface and where the satellite gravity field recovery is insufficient. These regions will include the areas surrounding the pole not covered by the satellite missions as well as many mountainous and ice-covered regions. The long wavelength of the satellite gravity field recovery will limit the effectiveness of spaced-based data for regional studies.

The resolution of airborne gravity indicates it is best applied to studies where the wavelengths of interest are from 5.5 to 400 km. The longer wavelengths will be effectively recovered by satellite missions while 5 km is presently the lowest wavelength routinely recovered from airborne gravity systems. Aircraft speed is the primary limit on the short wavelength anomaly recovery. For signals with wavelengths shorter than 5.5 km, a slower vehicle such as a helicopter or an airship would be required.

The accuracy of these airborne gravity data can be estimated from either evaluation of crossover error (2.98 mGal) or evaluation of repeat measurements (1.39 mGal). The accuracy of airborne gravity is currently limited by reliable recovery of the vertical positions and accelerations with GPS and possible inherent difficulties with the platforms which have been designed primarily for marine rather than airborne use.

References

Behrendt, J.C., W.E. LeMasurier, A.K. Cooper, F. Tessensohn, A. Trehu, and D. Damaske, The West Antarctic rift system - A review of geophysical investigations, in *Contributions to Antarctic Research II*, vol. 53, edited by D. H. Elliot, 67-112, AGU, Washington D.C., 1991.

Bell Aerospace Textron, Operation and maintenance manual for the gravity sensor subsystem BGM-3, Buffalo, New York, 1978.

Bell, R.E., J.M. Brozena, W.F. Haxby, and J.L. LaBrecque, Continental margins of the western Weddell Sea: Insights from airborne gravity and Geosat-derived gravity, in *Contributions to Antarctic Research I*, vol. 50, edited by D. H. Elliot, 91-102, AGU, Washington, D.C., 1990.

Bell, R.E., B. J. Coakley, and R. W. Stemp, Airborne gravimetry from a small twin engine aircraft over the Long Island Sound, *Geophysics*, 56(9), 1486-1493, 1991.

Bell, R.E., B.J. Coakley, D.D. Blankenship, S.M. Hodge, J.M. Brozena, and J. Jarvis, Airborne gravity from a light aircraft: CASERTZ 1990-1991, in *Recent Progress in Antarctic Earth Science*, edited by Y. Yoshida, K. Kaminuma, and K. Shiraishi, pp. 571-577, Terra Sci., Tokyo, 1992.

Bell, R.E., D.D. Blankenship, C.A. Finn, D.L. Morse, T.A. Scambos, J.M. Brozena, and S.M. Hodge, Influence of subglacial geology on the onset of a West Antarctic ice stream from aerogeophysical observations, *Nature*, 394, 58-62, 1998.

Blankenship, D.D., R.E. Bell, S.M. Hodge, J.M. Brozena, J.C. Behrendt, and C.A. Finn, Active volcanism beneath the West Antarctic ice sheet and implications for ice sheet stability, *Nature*, 361, 526-529, 1993.

Brozena, J.M., A preliminary analysis of the NRL airborne gravimetry system, *Geophysics*, 49(7), 1060-1069, 1984.

Brozena, J.M., Kinematic GPS and aerogeophysical measurement: Gravity, topography and magnetics, Ph. D. thesis, Cambridge Univ., Cambridge, U.K., 1995.

Brozena, J.M., G.L. Mader, and M.F. Peters, Interferometric Global Positioning System: Three-dimensional positioning source for airborne gravimetry, *J. Geophys. Res.*, 94(B9), 12,153-12,162, 1989.

Brozena, J.M., J. L. Jarvis, R. E. Bell, D.D. Blankenship, S. M. Hodge, and J.C. Behrendt, CASERTZ 91-92: Airborne gravity and surface topography measurement, *Antarct. J.*, 28, 1-3, 1993.

Childers, V.A., Gravimetry as a geophysical tool: Airborne gravimetry and studies of lithospheric flexure and faulting, Ph. D. thesis, Columbia Univ., New York, 1996.

Cooper, A.K., F.J. Davey, and K. Hinz, Crustal extension and origin of sedimentary basins beneath the Ross Sea and Ross Ice shelf, Antarctica, in *Geological Evolution of Antarctica*, edited by M.R.A. Thomson, J.A. Crame, and J.W. Thomson, pp. 285-292, Cambridge Univ. Press, New York, 1991.

Dalziel, I.W.D., and D.H. Elliot, West Antarctica: Problem child of Gondwanaland, *Tectonics*, 1, 3-19, 1982.

Drewry, D.J., *Antarctica: Glaciological and Geophysical Folio*, 9 pp., Cambridge Univ., Scott Polar Research Institute, Cambridge, U.K., 1983.

Gumert, W.R., Third generation aerogravity system, paper presented at International Symposium on Kinematic Systems in Geodesy, Geomatics, and Navigation, Int. Union of Geophys. and Geod., Boulder, Colo., 1995.

Harlan, R.B., Eötvös corrections for airborne gravimetry, *J. Geophys. Res.*, 73, 4675-4679, 1968.

Harrison, J.C., J.D. MacQueen, A.C. Rauhut, and J.Y. Cruz, The LCT airborne gravity system, paper presented at International Symposium on Kinematic Systems in Geodesy, Geomatics, and Navigation, Int. Union of Geophys. and Geod., Boulder, Colo., 1995.

King, R.W., and Y. Bock, Documentation for the MIT GPS analysis software: GAMIT, vol. 9.71, Mass. Inst. of Technol., Cambridge, U.K., 1993.

LaCoste, L.J.B., Measurement of gravity at sea and in the air, *Rev. Geophys.*, 5(4), 477-526, 1967.

Mader, G.L., Dynamic positioning using GPS carrier phase measurements, *Manuscr. Geod.*, 11, 272-277, 1986.

National Research Council, *Airborne Geophysics and Precise Positioning: Scientific Issues and Future Directions*, 111 pp., Nat. Acad. Press, Washington, D.C., 1995.

Peyton, D.R., An investigation into acceleration determination for airborne gravimetry using the Global Positioning System, M.Sc.E. thesis, Dept. of Surveying Engineer. Tech. rep. no. 149, 140 pp., Univ. of New Brunswick, Fredericton, New Brunswick, Canada, 1990.

Robertson, J.D., C.R. Bentley, J.W. Clough, and L.L. Greischar, Sea-bottom topography and crustal structure below the Ross Ice Shelf, Antarctica, in *Antarctic Geoscience - Symposium on Antarctic Geology and Geophysics*, edited by C. Craddock, pp. 1083-1090, Univ. of Wis. Press, Madison, 1982.

Rose, K.E., Radio echo studies of bedrock in southern Marie Byrd Land, Antarctica, in *Antarctic Geoscience - Symposium on Antarctic Geology and Geophysics*, edited by C. Craddock, pp. 985-992, Univ. of Wis. Press, Madison, 1982.

Skou, N., and F. Sondergaard, Radioglaciology: A 60 MHz Ice Sounder System, rep. R169, 124pp., Electromagnetics Inst., Tech. Univ. of Denmark, Lyngby, 1976.

Smith, W.H.F., and P. Wessel, Gridding with continuous curvature splines in tension, *Geophysics*, 55, 293-305, 1990.

Turcotte, D.L., and G. Schubert, *Geodynamics*, 450 pp., John Wiley, New York, 1982.

Webb, F.H., and J.F. Zumberge, An introduction to GIPSY/OASIS II, Jet Propulsion Laboratory Internal Document D-11088, Calif. Instit. of Tech., Pasadena, 1993.

Wessel, P., XOVER: A crossover error detector for track data, *Comput. Geosci.*, 15, 333-346, 1989.

Wilson, T.J., Mesozoic and Cenozoic kinematic evolution of the Transantarctic Mountains, in *Recent Progress in Antarctic Earth Science*, edited by K. Kaminuma and Y. Yoshida, pp. 304-314, Terra Sci., Tokyo, 1992.

Wilson, T.J., Cenozoic transtension along the Transantarctic Mountains, West Antarctic rift boundary, South Victoria Land, Antarctica, *Tectonics*, 14, 531-545, 1995.

R. A. Arko and R. E. Bell, Lamont-Doherty Earth Observatory of Columbia University, 61 Route 9W, Palisades, NY 10964. (arko@ldeo.columbia.edu; robinb@ldeo.columbia.edu)

D. D. Blankenship, Institute for Geophysics, University of Texas, 4412 Spicewood Springs Road, Austin, TX 78759. (blank@ig.utexas.edu)

J. M. Brozena and V. A. Childers, Naval Research Laboratory, Code 7420, 4555 Overlook Avenue, SW, Washington, DC 20375. (john@qur.nrl.navy.mil; vicki@qur.nrl.navy.mil)